

Rotation of Triangular Vortex Lattice in the Two-Band Superconductor MgB₂

Tomoya HIRANO, Kenta TAKAMORI, Masanori ICHIOKA, and Kazushige MACHIDA

Department of Physics, Okayama University, Okayama 700-8530, Japan

To identify the contributions of the multiband nature and the anisotropy of a microscopic electronic structure to a macroscopic vortex lattice morphology, we develop a method based on the Eilenberger theory near H_{c2} combined with the first-principles band calculation to estimate the stable vortex lattice configuration. For a typical two-band superconductor MgB₂, successive transitions of vortex lattice orientation that have been observed recently by small angle neutron scattering [Das, *et al.*: Phys. Rev. Lett. **108** (2012) 167001] are explained by the characteristic field-dependence of two-band superconductivity and the competition of sixfold anisotropy between the σ - and π -bands. The reentrant transition at low temperature reflects the Fermi velocity anisotropy of the σ -band.

KEYWORDS: vortex lattice morphology, two-band superconductivity, MgB₂, first-principles band calculation, quasi-classical Eilenberger theory

Since vortices are self-forming objects in mixed states of type-II superconductors under applied magnetic fields, the properties of the vortex states give us valuable information on the characteristics of each superconductor. Among them, the vortex lattice morphology, depending on the temperature T and magnetic field H , is closely related to the anisotropy of the superconductivity. For example, reflecting the fourfold symmetric structure of a superconducting gap or the Fermi velocity in momentum space, the vortex lattice shows a gradual transformation from a triangular vortex lattice at low fields to a square lattice at high fields.¹ The anomalous vortex lattice transformation in a superconductor Nb, including a scalene triangular lattice, is considered to be a result of the anisotropy of the Fermi surface structure.²⁻⁴ For a reliable theoretical estimation of the vortex lattice morphology, we need microscopic calculations such as the use of the Eilenberger theory, beyond the phenomenological ones of the extended Ginzburg-Landau (GL) theory^{4,5} or the nonlocal London theory.⁶ Furthermore, to accurately consider the anisotropy of the Fermi surface structure, it is preferable that the results of first-principles band calculation for electronic states, such as density functional theory (DFT), are combined in the estimation of a stable vortex lattice. This theoretical approach was carried out in a study of the vortex lattice morphology in Nb.³ The success encouraged us to further extend the vortex physics along this line.

The properties of a superconductor MgB₂ as a typical multiband superconductor also attract much attention. The superconductivity in MgB₂ consists of the σ -band with a large superconducting gap and the π -band with a small gap.^{7,8} In the vortex state, there are some interesting phenomena reflecting the multiband superconductivity, such as a rapid increase in the H -dependence of low-temperature specific heat $C(H) = \gamma(H)T$ at low fields,⁹⁻¹³ and the vortex clustering of the so-called type 1.5 superconductivity at low fields.¹⁴ Also, an interesting vortex lattice morphology has recently been reported in MgB₂ for $H \parallel c$.^{15,16} Since the crystal lattice is hexagonal, a triangular vortex lattice is formed in MgB₂. As schematically shown in Fig. 1, from small angle neutron scattering (SANS) experiments,¹⁶ the orientation of the triangular vortex lattice is $\phi = 0^\circ$ (F-phase) at low fields, and $\phi = 30^\circ$

(I-phase) at high fields, where ϕ is the angle measured from the a^* -axis in real space (a -axis in reciprocal space) of the underlying hexagonal crystal. In the intermediate fields, the orientation rotates gradually between $0^\circ < \phi < 30^\circ$ (L-phase). However, at low- T , the high-field I-phase reported in a previous work¹⁵ has been confirmed as a metastable state in a more recent work.¹⁶ The true stable state at low- T and high fields is found to be L-phase, as shown in Fig. 1. Therefore, a stable vortex lattice shows the successive transition $L \rightarrow I \rightarrow L \rightarrow F$ along H_{c2} upon raising T from $T = 0$ to the transition temperature T_c . In a previous study based on phenomenological GL theory,⁵ the transition $I \rightarrow L \rightarrow F$ was considered as a result of competition in anisotropies between the σ -band and the π -band in two-band superconductivity. However, the reentrant transition $L \rightarrow I$ at low- T has not yet been explained theoretically. We note that the original GL theory is valid only near T_c . To discuss the vortex morphology of MgB₂, we have to consider the 6th- and 12th-order derivative terms for gradient terms of the GL equation. The nonlocal correction terms of the $2n$ -th order derivative are on the order of $(1 - T/T_c)^{n-1}$. Thus, it is difficult in the framework of the GL theory to discuss the vortex morphology in the low-temperature region, because we need further higher-order derivative correction terms. On the other hand, since the Eilenberger theory can be applied to all T regions, we can obtain a reliable estimation for a vortex structure including that in a low- T region. The purpose of this study is to investigate the successive transition of $L \rightarrow I \rightarrow L \rightarrow F$ along H_{c2} , on the basis of the Eilenberger theory of two-band superconductors combined with DFT calculation¹⁷ to consider the Fermi surface of MgB₂.

First, we study the sixfold anisotropy of the Fermi surface structure in MgB₂. The electronic state of MgB₂ is evaluated by DFT calculation¹⁷ using local density approximation and the lattice constants $a = b = 3.083\text{\AA}$, and $c = 3.521\text{\AA}$.¹⁸ We chose the muffin-tin radii R_{MT} of 2.35 and 1.67 a.u., respectively, and use a plane-wave cutoff $R_{\text{MT},\text{min}}K_{\text{max}} = 9.0$. The first Brillouin zone is divided into $120 \times 120 \times 90$ grids. By the tetrahedron method¹⁹ for determining patches of the Fermi surface from the grids, we estimate the Fermi wave number \mathbf{k}_i , Fermi velocity $\mathbf{v}_i = (v_{i,x}, v_{i,y}, v_{i,z})$, and Fermi surface DOS $D_i(\epsilon_F)$ on the i -th patch of the Fermi surface.

arXiv:1304.7314v1 [cond-mat.supr-con] 27 Apr 2013

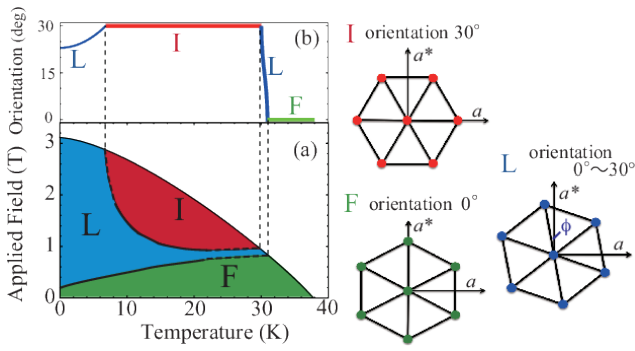


Fig. 1. (Color online) (a) Schematic phase diagram of vortex lattice morphology as a function of H and T , obtained by the SANS experiment.¹⁶ The phase boundary near H_{c2} is extrapolated. Triangular lattices in the right panel show the orientation ϕ of each-phase. (b) The T dependence of ϕ is schematically presented along H_{c2} .

As shown in Fig. 2(a), our calculation reproduces the well-known Fermi surfaces of the σ -band and the π -band.²⁰ For later discussions on the reasons for the vortex lattice morphology in MgB_2 , we study the anisotropy of the Fermi velocity projected within the xy plane perpendicular to the applied field along the z -direction. The color on the Fermi surfaces in Fig. 2(a) shows the orientation angle φ_{v_i} of the Fermi velocity defined as $\tan \varphi_{v_i} = v_{i,y}/v_{i,x}$. Figures 2(b) and 2(c) show the φ_v -resolved Fermi surface DOS defined as

$$D_m(\varphi_v) = \langle \delta(\varphi_v - \varphi_{v_i}) \rangle_m, \quad (1)$$

for each band ($m = \sigma, \pi$), where the band-resolved Fermi surface average is $\langle \cdots \rangle_m = \sum_{i \in m} D_i(\epsilon_F) (\cdots)$. As shown in Fig. 2(b), the Fermi surfaces of the σ -band are two hexagonal cylinders rather than circular ones. Most of the Fermi velocity on the flat surface is oriented to 30° or equivalent directions. The Fermi surface of the π -band is also flat, and most of the Fermi velocity on the flat surface is oriented to 0° or equivalent directions, as shown in Fig. 2(c). Therefore, the $D_m(\varphi_v)$ values of the Fermi surface are different between the two bands, inducing a competition between the F and I phases for the vortex lattice orientation, as will be discussed later. The ratio of the Fermi surface DOS of the π -band to the σ -band is calculated to be $N_\pi/N_\sigma = 1.36$, indicating that the π -band contribution is larger.

Next, we explain our formulation for estimating the stable vortex lattice configuration, which is extended to two-band superconductors in this work. To shorten our calculation within a reasonable computational time even when we consider the detailed structure of three-dimensional Fermi surfaces, our study of the stable vortex lattice is restricted near H_{c2} , as a first approach to this problem. We assume an isotropic s-wave superconducting gap in each band, and a clean limit.

Quasi-classical Green's functions $g(\omega_n, \mathbf{k}_i, \mathbf{r})$, $f(\omega_n, \mathbf{k}_i, \mathbf{r})$, and $f^\dagger(\omega_n, \mathbf{k}_i, \mathbf{r})$ with a Matsubara frequency ω_n are defined at \mathbf{k}_i on each Fermi surface. They are calculated by the Eilenberger equation^{13,21}

$$\{\omega_n + \mathbf{v}_i \cdot (\nabla + i\mathbf{A})\} f(\omega_n, \mathbf{k}_i, \mathbf{r}) = \Delta_m(\mathbf{r}) g(\omega_n, \mathbf{k}_i, \mathbf{r}) \quad (2)$$

and the equivalent equation for f^\dagger , where $g = (1 - ff^\dagger)^{1/2}$ and \mathbf{A} is the vector potential. Throughout this letter, we use Eilenberger units,²² i.e., energy, temperature, and length are

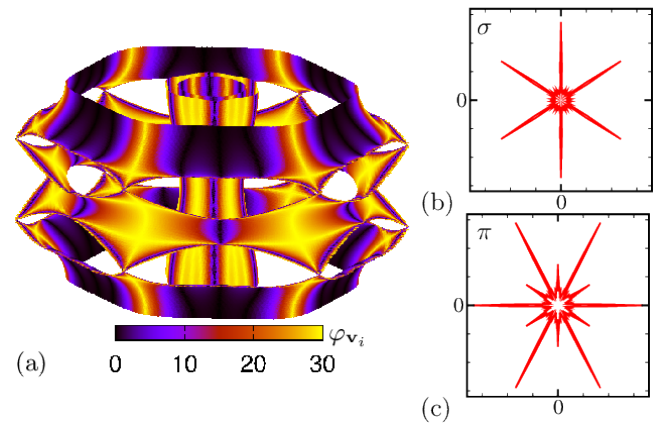


Fig. 2. (Color online) (a) Fermi surfaces of MgB_2 obtained in our calculation. The two cylinders in the center are the σ -band's Fermi surface, and the outside rings are the π -band's Fermi surfaces. The color on the surface indicates the orientation φ_{v_i} (mod 30°) of the Fermi velocity. (b) φ_v -resolved Fermi surface DOS $D_\sigma(\varphi_v)$ for the σ -band. (c) $D_\pi(\varphi_v)$ for the π -band. In (b) and (c), we plot lines of $(D_m(\varphi_v) \cos \varphi_v, D_m(\varphi_v) \sin \varphi_v)$ for $0 \leq \varphi_v \leq 360^\circ$ ($m = \sigma, \pi$), so that the distances from the center to the lines indicate $D_m(\varphi_v)$.

in units of $\pi k_B T_c$, T_c , and $\xi_0 = \hbar v_F / 2\pi k_B T_c$, respectively. The self-consistent gap equation for the pair potential $\Delta_m(\mathbf{r})$ of m -bands ($m = \sigma, \pi$) is given by

$$\begin{pmatrix} \Delta_\sigma(\mathbf{r}) \\ \Delta_\pi(\mathbf{r}) \end{pmatrix} = \hat{V} T \sum_{\omega_n} \begin{pmatrix} \langle f(\omega_n, \mathbf{k}_i, \mathbf{r}) \rangle_\sigma \\ \langle f(\omega_n, \mathbf{k}_i, \mathbf{r}) \rangle_\pi \end{pmatrix}. \quad (3)$$

As for the interaction constants of superconductivity,

$$\hat{V} = \begin{pmatrix} V_{\sigma,\sigma} & V_{\sigma,\pi} \\ V_{\sigma,\pi} & V_{\pi,\pi} \end{pmatrix}, \quad (4)$$

where $V_{\sigma,\sigma}$ ($V_{\pi,\pi}$) is the pairing interaction in the σ - (π -) band, and $V_{\sigma,\pi}$ is the Cooper pair transfer between two bands. We have to select these parameters under the condition to reproduce the gap ratio $\Delta_\pi/\Delta_\sigma = \frac{1}{4} \sim \frac{1}{2}$ observed in experiments.⁸ Previous first-principles band calculation²³ estimated (i) $V_{\sigma,\pi} = 0.15V_{\sigma,\sigma}$ and $V_{\pi,\pi} = 0.32V_{\sigma,\sigma}$. These are used in our calculations. We determine $V_{\sigma,\sigma}$ from the gap equation at $T = T_c$.

We expand $\Delta_m(\mathbf{r})$ and $f(\omega_n, \mathbf{k}_i, \mathbf{r})$ in terms of the Landau-Bloch function $\psi_{N,\mathbf{q}}(\mathbf{r})$,^{24,25} whose the N -th coefficients of the Landau level are $\Delta_{m,N}$ and $f_N(\omega_n, \mathbf{k}_i)$. The vortex lattice configuration is determined by the parameters of $\psi_{N,\mathbf{q}}(\mathbf{r})$, and the relative angle of the crystal coordinate and vortex coordinate. Along H_{c2} where $g \rightarrow \text{sgn} \omega_n$, the Eilenberger equation (2) is reduced to^{24,25}

$$f_N(\omega_n, \mathbf{k}_{i \in m}) = \sum_M (\mathcal{M}^{-1})_{N,M} \Delta_{m,M} \quad (5)$$

with $\mathcal{M}_{N,M} = |\omega_n| \delta_{N,M} + \sqrt{N+1} b^* \delta_{N,M-1} - \sqrt{N} b \delta_{N,M+1}$ and $b = (v_{i,x} + i v_{i,y}) \text{sgn}(\omega_n) \sqrt{H} / (2\sqrt{2})$. The Fermi velocities $v_{i,x}$ and $v_{i,y}$ at \mathbf{k}_i , appearing in b , determine the \mathbf{k}_i dependence of f_N . Therefore, at $B = H_{c2}$, the gap equation (3) is reduced to

$$\begin{pmatrix} \Delta_{\sigma,N} \\ \Delta_{\pi,N} \end{pmatrix} = \hat{V} T \sum_{\omega_n} \sum_M \begin{pmatrix} \langle (\mathcal{M}^{-1})_{N,M} \rangle_\sigma \Delta_{\sigma,M} \\ \langle (\mathcal{M}^{-1})_{N,M} \rangle_\pi \Delta_{\pi,M} \end{pmatrix}. \quad (6)$$

In the Eilenberger theory, the free energy in a two-band superconductor is given by $F = \kappa^2 B^2 + F_{c1} + F_{c2}$ with the GL

parameter κ and

$$F_{c1} = \sum_{n,m=\sigma,\pi} \overline{\Delta_n^*(\mathbf{r})(\hat{V}^{-1})_{n,m}\Delta_n(\mathbf{r})}, \quad (7)$$

$$F_{c2} = -T \sum_{\omega_n} \sum_m \overline{\langle I \rangle_m}, \quad (8)$$

where $\overline{(\dots)}$ indicates the spatial average and $I = (g - \text{sgn}\omega_n)[2\omega_n + \mathbf{v}_i \cdot (\nabla \ln(f/f^\dagger) + 2i\mathbf{A})] + f\Delta^* + \Delta f^\dagger$. Using the gap equation (3), we obtain

$$F_{c1} = \frac{T}{2} \sum_{\omega_n} \sum_m \overline{(\Delta_m \langle f^\dagger \rangle_m + \Delta_m^* \langle f \rangle_m)}. \quad (9)$$

Since the condensation energy part $F_{c1} + F_{c2}$ is a simple summation of each band contribution, the derivation of free energy near H_{c2} can be performed as in a single band case,^{26–28} as follows. We substitute $g \sim 1 - ff^\dagger/2 - (ff^\dagger)^2/8$ in F and set $\mathbf{A} = \mathbf{A}_{c2} + \mathbf{A}_1$, where $\nabla \times \mathbf{A}_{c2} = \mathbf{H}_{c2}$, $\nabla \times \mathbf{A}_1 = \mathbf{h}_1$, and $\mathbf{h}_1 = \mathbf{H} - \mathbf{H}_{c2} + \mathbf{h}_s$ for an applied field H near H_{c2} . Thus, the Abrikosov identity²⁷ is derived as

$$T \sum_{\omega_n > 0} \sum_m \overline{\langle ff^\dagger(\Delta_m f^\dagger + \Delta_m^* f) \rangle_m} - 4\kappa^2 \overline{\mathbf{h}_1 \cdot \mathbf{h}_s} = 0, \quad (10)$$

where \mathbf{h}_s is the magnetic field induced by supercurrent, and

$$\nabla \times \mathbf{h}_s = \frac{T}{\kappa^2} \sum_{\omega_n > 0} \sum_m \langle \mathbf{v} f f^\dagger \rangle_m. \quad (11)$$

Finally, we obtain the free energy at magnetic induction $B = H + \bar{h}_s$ near H_{c2} as²⁶

$$\frac{F}{\kappa^2} = B^2 - \frac{(B - H_{c2})^2}{\mathcal{F}' + 1}, \quad (12)$$

with

$$\mathcal{F}' = \frac{T}{4\kappa^2 \bar{h}_s^2} \sum_{\omega_n > 0} \sum_m \overline{\langle f f^\dagger (\Delta_m f^\dagger + \Delta_m^* f) \rangle_m} - \frac{\bar{h}_s^2}{\bar{h}_s^2}. \quad (13)$$

Since we consider the case $\kappa \gg 1$ here, the last term with \bar{h}_s^2 in Eq. (13) is neglected. The free-energy minimum corresponds to the minimum of \mathcal{F}' .

Using $D_i(\epsilon_F)$ and \mathbf{v}_i obtained by the DFT calculation above, we solve the gap equation (6) of matrix form and obtain H_{c2} and Δ_m at a given T . Substituting Δ_m to Eq. (5) we obtain quasi-classical Green's function f . By these Δ_m and f , we calculate \mathcal{F}' in Eq. (13). These calculations are performed for possible orientations ($0^\circ \leq \phi \leq 30^\circ$) of the triangular vortex lattice, and we determine the stable orientation of the vortex lattice along the H_{c2} line, by the free-energy minimum.

In Fig. 3(a), we show $\mathcal{F}'(\phi)/\mathcal{F}'(\phi = 0)$ as a function of ϕ at some T values. There, \mathcal{F}' has a minimum at $\phi = 0^\circ$ for $T \geq 0.913$. That is, the F-phase is stable at high- T and low- H near T_c . For $0.908 < T/T_c < 0.913$, the minimum orientation ϕ changes gradually from 0 to 30° , indicating that the L-phase is stable. For $0.46 \leq T/T_c \leq 0.908$ at higher fields, the I-phase of $\phi = 30^\circ$ is stable. The T dependence of the stable orientation ϕ is presented in Figs. 3(b) and 3(c). At a low temperature $T/T_c < 0.48$ at high fields, we see the reentrant transition to the L-phase where ϕ decreases from 30° . These successive transitions of the vortex lattice, i.e., $L \rightarrow I \rightarrow L \rightarrow F$ from a low- T along H_{c2} , qualitatively reproduce the phase diagram observed in the SANS experiment.¹⁶ Interestingly, we note

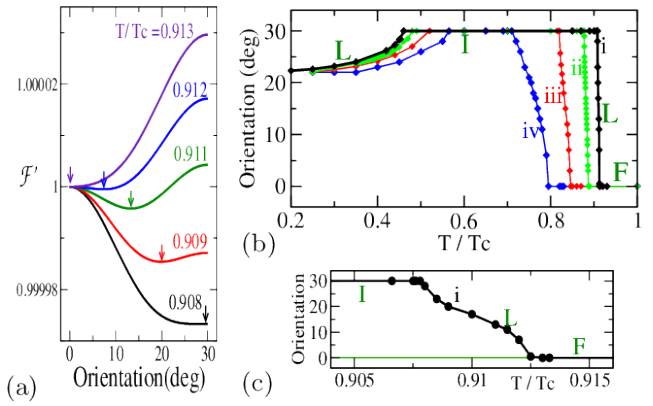


Fig. 3. (Color online) (a) $\mathcal{F}'(\phi)/\mathcal{F}'(\phi = 0)$ as a function of ϕ at $T/T_c = 0.908, 0.909, 0.911, 0.912$, and 0.913 , showing transition $I \rightarrow L \rightarrow F$, for (i) $V_{\sigma,\pi} = 0.15V_{\sigma,\sigma}$, $V_{\pi,\pi} = 0.32V_{\sigma,\sigma}$. The intervals of data points are 1° along each line. Arrows indicate the minimum of each line. (b) Stable orientation ϕ of triangular vortex lattice as a function of T/T_c along H_{c2} line. In addition to case (i), we also show lines for (ii) $V_{\sigma,\pi} = V_{\sigma,\sigma}/3$, $V_{\pi,\pi} = 0$, (iii) $V_{\sigma,\pi} = V_{\sigma,\sigma}/2$, $V_{\pi,\pi} = 0$, and (iv) $V_{\sigma,\pi} = V_{\sigma,\sigma}/3$, $V_{\pi,\pi} = V_{\sigma,\sigma}/2$. (c) The high- T range of the transition $I \rightarrow L \rightarrow F$ of (i) is focused on.

that data points at the lowest T (2 K) and high field (1.8 T) show $\phi \sim 23^\circ$,¹⁶ which nicely correspond to our result of ϕ at the lowest T in Fig. 3(b).

To confirm that these qualitative results in Fig. 3(b) do not strongly depend on the interaction parameters within appropriate values for MgB₂, we show stable orientations also in other cases (ii) $V_{\sigma,\pi} = V_{\sigma,\sigma}/3$, $V_{\pi,\pi} = 0$, (iii) $V_{\sigma,\pi} = V_{\sigma,\sigma}/2$, $V_{\pi,\pi} = 0$, and (iv) $V_{\sigma,\pi} = V_{\sigma,\sigma}/3$, $V_{\pi,\pi} = V_{\sigma,\sigma}/2$. The gap ratios are $\Delta_\pi/\Delta_\sigma = 0.24$ (i), 0.29 (ii), 0.40 (iii), and 0.57 (iv). We see similar successive transitions there, and find that the range of the F-phase (I-phase) becomes wider (narrower) with the increase in Δ_π/Δ_σ . This indicates that the stability of the F-phase is due to the contribution of the π -band.

To clarify the contributions of the two bands, which are competing with each other, we evaluate the stable orientation of each band. As shown in Fig. 4, if we assume that only the σ -band is superconducting ($V_{\sigma,\pi} = V_{\pi,\pi} = 0$), the stable vortex lattice is the I-phase with $\phi = 30^\circ$ at $T \geq 0.45T_c$, reflecting the Fermi velocity anisotropy in Fig. 2(b). Namely, the nearest neighbor of vortices is oriented in the direction where $D_\sigma(\varphi_v)$ is small. At a lower T and a higher H along H_{c2} , ϕ decreases from 30° , changing to the L-phase. On the other hand, if we assume that only the π -band is superconducting ($V_{\sigma,\pi} = V_{\sigma,\sigma} = 0$), we obtain opposite results, reflecting the opposite Fermi velocity anisotropy in Fig. 2(c). That is, the stable vortex lattice is the F-phase with $\phi = 0^\circ$ at $T \geq 0.65T_c$, which changes to the L-phase with increasing ϕ from 0° at a low T . The reason why the vortex lattice orientation moves at a low T along H_{c2} in both cases is the Fermi velocity anisotropy changing its contributions at high fields. That is, the anisotropy in the σ (π)-band contributes to stabilize the I- (F-) phase at low fields, but makes the low-field-phase unstable at high fields. This effect is also seen in the case of a square vortex lattice of four-fold symmetric superconductors.¹ To discuss the reason for these behaviors, we consider the β -model of the cylindrical Fermi surface.¹ If we assume sixfold anisotropy $|\mathbf{v}_i| \propto 1 + 0.4 \cos 6\varphi_v$ for the Fermi velocity in Eq. (2), the stable orientation is at 0° . Instead, if we assume anisotropy $D_i(\epsilon_F) \propto 1/(1 + 0.4 \cos 6\varphi_v)$ for the Fermi

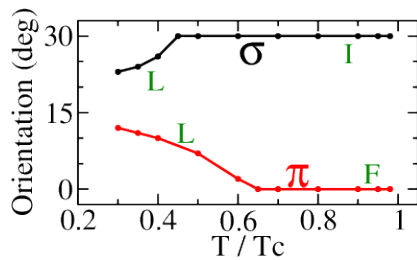


Fig. 4. (Color online) Stable orientation ϕ as a function of T/T_c along H_{c2} line when only the σ -band is superconducting ($V_{\sigma,\pi} = V_{\pi,\pi} = 0$) and when only the π -band is superconducting ($V_{\sigma,\pi} = V_{\sigma,\sigma} = 0$).

surface DOS, the stable orientation is at 30° . Combining both anisotropies of \mathbf{v}_i and $D_i(\epsilon_F)$, the stable orientation is at 0° at low fields, and changes to 30° at high fields. Since there is usually the relation $D_i(\epsilon_F) \propto 1/|\mathbf{v}_i|$, the anisotropies of \mathbf{v}_i and $D_i(\epsilon_F)$ tend to compete with each other, inducing the change of stable orientation between low fields and high fields.

On the basis of the results in Fig. 4, we discuss the origin of the phase diagram of the vortex lattice presented in Fig. 3(b). The F-phase near T_c is given by the contribution of the π -band, since the total DOS N_π and the anisotropy of the π -band is large compared with that of the σ -band, as discussed in Fig. 2. However, the contribution of the π -band decreases at high fields, since the superconductivity in the π -band becomes normal-state-like there.^{7,13} This is because the effective upper-critical field of the π -band is smaller than that of the σ -band, which is roughly proportional to the gap amplitude Δ_π/Δ_σ . Thus, since the effective upper-critical field decreases for (iv) \rightarrow (iii) \rightarrow (ii) \rightarrow (i), the π -band contributions becomes weaker in this order in Fig. 3(b). The I-phase appears at low- T and high fields, owing to the contributions of the σ -band. Therefore, the transition I \rightarrow L \rightarrow F in the high- T region occurs owing to the competition of sixfold anisotropy between the two bands. The low- T reentrant behavior from the I-phase to the L-phase in Fig. 3(b) is due to the anisotropy of the σ -band. The reentrance to the L-phase occurs similarly in the vortex lattice behavior of the σ -band in Fig. 4.

When our results are compared with those in experimental observation,¹⁶ it is noted that the phase boundaries in Fig. 1 are extrapolated near H_{c2} . The weak anisotropy of the s -wave superconducting gap and impurity scattering, which are not considered in this study, may be factors of minor quantitative modification for our theoretical estimation of a stable vortex lattice configuration.

A recent SANS experiment²⁹ on CaAlSi, which has the same AIB₂-type crystal structure and a similar two-band feature,³⁰ has shown a first-order orientation transition of the vortex lattice. The present methodology is readily applicable to this and other omnipresent multiband superconductors, such as Fe pnictides.

In summary, a method for the microscopic Eilenberger analysis of a stable vortex lattice configuration along H_{c2} combined with the first-principles band calculation of DFT is developed for a two-band superconductor. We apply this new formulation to MgB₂, and explain the successive transition¹⁶ L \rightarrow I \rightarrow L \rightarrow F in the orientation of a triangular vortex lattice, by properly considering the Fermi surface anisotropy of the two bands. This successful endeavor establishes a method

using the first-principles band calculation to obtain valuable information on the multiband and anisotropy of superconductivity from the vortex lattice configuration and morphology. We hope that this approach will be applied to other superconductors in future studies.

We thank M.R. Eskildsen for stimulating discussions and information on their experimental results. We also acknowledge useful discussions with P. Miranović, N. Nakai, and H.M. Adachi for the formulation and calculation methods. This work was supported by KAKENHI No. 21340103.

- 1) K. M. Suzuki, K. Inoue, P. Miranović, M. Ichioka, and K. Machida: J. Phys. Soc. Jpn. **79** (2010) 013702.
- 2) M. Laver, E. M. Forgan, S. P. Brown, D. Charalambous, D. Fort, C. Bowell, S. Ramos, R. J. Lycett, D. K. Christen, J. Kohlbrecher, C. D. Dewhurst, and R. Cubitt: Phys. Rev. Lett. **96** (2006) 167002.
- 3) H. M. Adachi, M. Ishikawa, T. Hirano, M. Ichioka, and K. Machida: J. Phys. Soc. Jpn. **80** (2011) 113702.
- 4) K. Takanaka: Prog. Theor. Phys. **50** (1973) 365.
- 5) M. E. Zhitomirsky and V.-H. Dao: Phys. Rev. B **69** (2004) 054508.
- 6) V. G. Kogan, P. Miranović, Lj. Dobrosavljević-Grujić, W. E. Pickett, and D. K. Christen: Phys. Rev. Lett. **79** (1997) 741.
- 7) R. S. Gonnelli, D. Daghero, G. A. Umbarino, V. A. Stepanov, J. Jun, S. M. Kazakov, and J. Karpinski: Phys. Rev. Lett. **89** (2002) 247004.
- 8) H. Schmidt, J. F. Zasadzinski, K. E. Gray, and D. G. Hinks: Physica C **385** (2003) 221.
- 9) H. D. Yang, J.-Y. Lin, H. H. Li, F. H. Hsu, C. J. Liu, S.-C. Li, R.-C. Yu, and C.-Q. Jin: Phys. Rev. Lett. **87** (2001) 167003.
- 10) F. Bouquet, R. A. Fisher, N. E. Phillips, D. G. Hinks, and J. D. Jorgensen: Phys. Rev. Lett. **87** (2001) 047001.
- 11) N. Nakai, M. Ichioka, and K. Machida: J. Phys. Soc. Jpn. **71** (2002) 23.
- 12) A. E. Koshelev and A. A. Golubov: Phys. Rev. Lett. **90** (2003) 177002.
- 13) M. Ichioka, K. Machida, N. Nakai, and P. Miranović: Phys. Rev. B **70** (2004) 144508.
- 14) V. Moshchalkov, M. Menghini, T. Nishio, Q. H. Chen, A. V. Silhanek, V. H. Dao, L. F. Chibotaru, N. D. Zhigadlo, and J. Karpinski: Phys. Rev. Lett. **102** (2009) 117001.
- 15) R. Cubitt, M. R. Eskildsen, C. D. Dewhurst, J. Jun, S. M. Kazakov, and J. Karpinski: Phys. Rev. Lett. **91** (2003) 047002.
- 16) P. Das, C. Rastovski, T. R. O'Brien, K. J. Schlessinger, C. D. Dewhurst, L. DeBeer-Schmitt, N. D. Zhigadlo, J. Karpinski, and M. R. Eskildsen: Phys. Rev. Lett. **108** (2012) 167001.
- 17) P. Blaha, K. Schwarz, G. Madsen, D. Kvasnicka, and J. Luitz: WIEN2k (Vienna Univ. Technology, Austria, 2001).
- 18) X. Wan, J. Dong, H. Weng, and D. Y. Xing: Phys. Rev. B **65** (2001) 012502.
- 19) P. E. Blöchl, O. Jepsen, and O. K. Andersen: Phys. Rev. B **49** (1994) 16223.
- 20) J. Kortus, I. I. Mazin, K. D. Belashchenko, V. P. Antropov, and L. L. Boyer: Phys. Rev. Lett. **86** (2001) 4656.
- 21) G. Eilenberger: Z. Phys. **214** (1968) 195.
- 22) U. Klein: J. Low Temp. Phys. **69** (1987) 1.
- 23) A. A. Golubov, J. Kortus, O. V. Dolgov, O. Jepsen, Y. Kong, O. K. Andersen, B. J. Gibson, K. Ahn, and R. K. Kremer: J. Phys.: Condens. Matter **14** (2002) 1353.
- 24) T. Kita and M. Arai: Phys. Rev. B **70** (2004) 224522.
- 25) T. Kita: J. Phys. Soc. Jpn. **67** (1998) 2067.
- 26) N. Nakai, P. Miranović, M. Ichioka, and K. Machida: Phys. Rev. Lett. **89** (2002) 237004.
- 27) A. A. Abrikosov: Zh. Eksp. Teor. Fiz. **32** (1957) 1442 [Sov. Phys. JETP **5** (1957) 1174].
- 28) P. G. de Gennes: *Superconductivity of Metals and Alloys* (Addison Wesley, CA, 1989) Sec. 6-7.
- 29) P. K. Biswas, M. R. Lees, G. Balakrishnan, D. Q. Liao, D. S. Keeble, J. L. Gavilano, N. Egetenmeyer, C. D. Dewhurst, and D. M. Paul: Phys. Rev. Lett. **108** (2012) 077001.
- 30) S. Kuroiwa, A. Nakashima, S. Miyahara, N. Furukawa, and J. Akimitsu: J. Phys. Soc. Jpn. **76** (2007) 113705.